Matrix Biology Plus 24 (2024) 100165

Contents lists available at ScienceDirect

Matrix Biology Plus

journal homepage: www.sciencedirect.com/journal/matrix-biology-plus

Investigation of neuro-regenerative therapeutic potential of nerve composite matrix hydrogels embedded with adipose-derived stem cells

Inha Baek, Younghye Song *

Department of Biomedical Engineering, University of Arkansas, Fayetteville, AR 72701, USA

ARTICLE INFO

Keywords:
Spinal cord injury
Decellularized tissue matrix
Hydrogel
Adipose-derived stem cells
Matrisome
Tissue engineering

ABSTRACT

Traumatic spinal cord injury (SCI) induces permanent sensorimotor deficit below the site of injury. There is various research conducted to provide effective therapy, however, SCI is still considered incurable due to the complex nature of the injury site. Recently, our lab developed a combinatorial therapeutic for SCI repair comprising human adipose-derived stem cell (hASC)-embedded nerve composite hydrogels using different ratios of decellularized sciatic nerve (dSN) and spinal cord (dSC) matrices. This study investigated angiogenic and neurotrophic effects of the combinatorial therapeutic in vitro. Compression testing was performed to analyze mechanical properties of the composite hydrogels and showed no significant difference between all hydrogel groups. Next, pro-angiogenic factors and neurotrophins secreted from hASCs within different ratios of the composite hydrogels were analyzed and we found culture durations and extracellular matrix (ECM) composition affect secretory behavior. Interestingly, ECM compositional difference between hydrogel groups had little influence on human brain microvascular endothelial cells (HBVECs) infiltration and dorsal root ganglia (DRG) neurite outgrowth. Finally, we conducted proteomic analysis to identify the ECM components potentially contributing to these observed effects. Taken together, dSN:dSC = 1:2 hydrogel showed slightly better therapeutic potentials, warranting validation using *in vivo* studies.

Introduction

Traumatic spinal cord injury (SCI) often leads to a permanent loss of motor and sensory function below the site of injury. SCI is particularly devastating due to a limited regenerative capacity of the central nervous system (CNS) [1]. SCI can result in a series of pathophysiological events including cell death, axonal degeneration, scarring, cyst cavitation, inflammation, etc. [2]. These events contribute to additional breakdown of extracellular matrix (ECM) and imbalance in the spinal cord microenvironment that is unfavorable for tissue restoration and axonal regeneration [3,4]. It is important to provide a regenerative microenvironment for axonal regeneration and functional recovery. To this end, a variety of biomaterials and cell-based combinatorial therapies have been studied to facilitate SCI repair. Yet, clinical success of combinatorial therapeutics remains limited and warrants further development.

Human adipose-derived stem cells (hASCs) have emerged as a promising candidate for cell-based therapy in SCI due to their regenerative factor secretion, easy harvest in high yield, multipotency with ability to differentiate into neurogenic lineages, and therapeutic potential demonstrated in early stage clinical trials [5–8]. For instance, a recent Phase I clinical trial of intrathecal injection of autologous hASCs showed promising results in terms of safety and improvement in sensorimotor functions [9]. Interestingly, patients had to be rotated side-to-back-to-side after ASC injection to ensure homogeneous ASC distribution. The injured spinal cord presents a hostile environment characterized by inflammation and a lack of essential nutrients, which hinders the survival and integration of transplanted ASCs [10]. Thus, it is important to provide an injectable supportive niche for hASCs that can maintain their viability and functionality.

Biomaterials have gained attention for SCI repair because they can provide physical matrix that neurons and endogenous repairing cells can adhere and remain functionally active [11]. Among various types of biomaterials, ECM-based hydrogels are an outstanding option due to their biocompatibility, biodegradability, and ability to facilitate tissue regeneration [12]. The ECM, a key component of tissue microenvironment, provides a 3D structural network and is a critical regulator of multiple physiological and pathological processes, including cell adhesion, migration, survival, differentiation, neuronal growth and synapse

* Corresponding author at: 125 ENGR, 790 W Dickson St, Fayetteville, AR 72701, USA.
E-mail addresses: inhabaek@uark.edu (I. Baek), yhsong@uark.edu (Y. Song).

https://doi.org/10.1016/j.mbplus.2024.100165
Received 25 June 2024; Received in revised form 22 October 2024; Accepted 11 November 2024
Available online 16 November 2024

formation [13–16]. In this context, decellularization allows acquisition of these pro-regenerative ECM cocktails as the process removes cellular and nuclear components while preserving the structural and functional ECM components.

Decellularized ECM (dECM) derived from various tissues such as spinal cord, brain, urinary bladder, optic nerve, and peripheral nerve have been investigated for its potential in the SCI repair [17–19]. However, hydrogels alone cannot replace lost cells after SCI and it is often challenging to precisely regulate their properties to achieve the desired responses [11]. Cell transplantation is one of the widely utilized SCI regenerative approaches over the years, however, it's difficult to mediate survival, integration, and differentiation of transplanted cells. Therefore, combinatorial approaches have gained attention to take advantages of both approaches.

dSN derived hydrogels and peripheral nerve grafts are known to promote axonal regeneration after SCI repair with the inherent regenerative capacity of the peripheral nervous system [20]. However, the major challenges, including rapid degradation and neurons failing to extend beyond the distal graft-host interface, limit their ability to provide the supportive condition needed for axonal regeneration after SCI [20,21]. Hydrogels made from dSCs retain spinal cord-specific ECM components, which can provide natural bioactive cues that can interact with cells in a way that other natural or synthetic hydrogels cannot recapitulate. For example, dSC hydrogels have been shown to promote neural stem/progenitor cell (NSPCs) viability, proliferation, and migration compared to dSN or collagen hydrogels due to the presence of spinal cord-specific ECM proteins and growth factors [22]. However, rapid degradation and cyst formation hindered long-term structural support [23]. Combining these two different tissue-derived hydrogels may provide synergistic effects by leveraging the unique properties of each ECM proteins, enhancing hydrogel properties, cellular response, and axonal regeneration outcomes.

Previously, we fabricated nerve composite hydrogels containing decellularized sciatic nerve (dSN) and spinal cord (dSC) [24]. Moreover, hASCs were encapsulated in the nerve composite hydrogels and 3D viability of the cells were investigated. However, no further studies were conducted in the context of SCI repair. Therefore, it is necessary to investigate the therapeutic effects, such as angiogenic and neurotrophic effects, of hASCs-embedded nerve composite hydrogels for SCI.

In this study, hASC-laden composite hydrogels were further characterized with hASC secretion of angiogenic and neurotrophic factors after 7- and 14-day cultures. In addition, angiogenic and neurotrophic effects were investigated by seeding and embedding human brain microvascular endothelial cells (HBVECs) and dorsal root ganglia (DRG), respectively. Lastly, proteomic analysis of dSN and dSC was performed to analyze the ECM components that might influence hASC behavior within the composite hydrogels. Overall, our study offers insights on how the dSN and dSC may impact hASCs behavior and suggests the best candidate for future *in vivo* studies or SCI repair.

Results

Hydrogel stiffness is not affected by the ratios of dSN:dSC

The mechanical properties of the composite hydrogels were investigated using compression testing. The stress–strain graph revealed a J-shaped curve with three distinct regions: the toe, the linear (elastic), and the failure (Fig. 1A). Calculated Young's Moduli were 344.80 ± 35.02 Pa, 293.69 ± 43.91 Pa, 358.18 ± 27.22 Pa, and 314.28 ± 22.07 Pa for dSN:dSC = 2:1, 1:1, 1:2, and dSC only hydrogels, respectively (Fig. 1B). The result showed that there is no significant difference across all hydrogel groups.

dSN:dSC = 1:2 hydrogel induces increased cytokines release by embedded hASCs over time

Analysis of secreted cytokines from hASCs embedded in different composite hydrogels was performed using Luminex assay. The amount of angiogenic and neurotrophic factors were normalized by DNA content and compared between two different time points, day 7 and day 14. There was an increasing trend in IL-8, HGF, Ang-1 and bFGF secretion over culture time across all hydrogel groups (Fig. 2A). In 2:1 hydrogel, bFGF and Ang-1 were significantly more secreted over time compared to IL-8 and HGF while the 1:1 hydrogel showed significantly increased secretion of bFGF, HGF, and Ang-1. In contrast, 1:2 and dSC only hydrogels demonstrated a comprehensive secretion profile with all analytes being significantly more secreted over time. A consistent trend was observed from the neurotrophic factors analysis (Fig. 2B). Although statistically not significant, secretion of GDNF across all hydrogel groups was trending towards an increase over the culture period. NT-3 was significantly more released from 2:1 hydrogel only while BDNF and β-NGF secretion were significantly elevated at day 14 compared to day 7 across all hydrogel groups.

Immediate seeding of human brain microvascular endothelial cells (HBVECs) promotes endothelial sprouting

To investigate the effect of hASC-laden nerve composite hydrogels on angiogenic sprouting in vitro, HBVECs were seeded atop hydrogels either immediately or after 7 days of pre-culture and co-cultured for another three days in invasion media (Fig. 3A,B, and Supplementary Fig. S1A). The numbers of lumens were not significantly different across all hydrogel groups (Fig. 3C). However, after immediate seeding of HBVECs, the average length of sprouts from 1:2 and dSC only groups

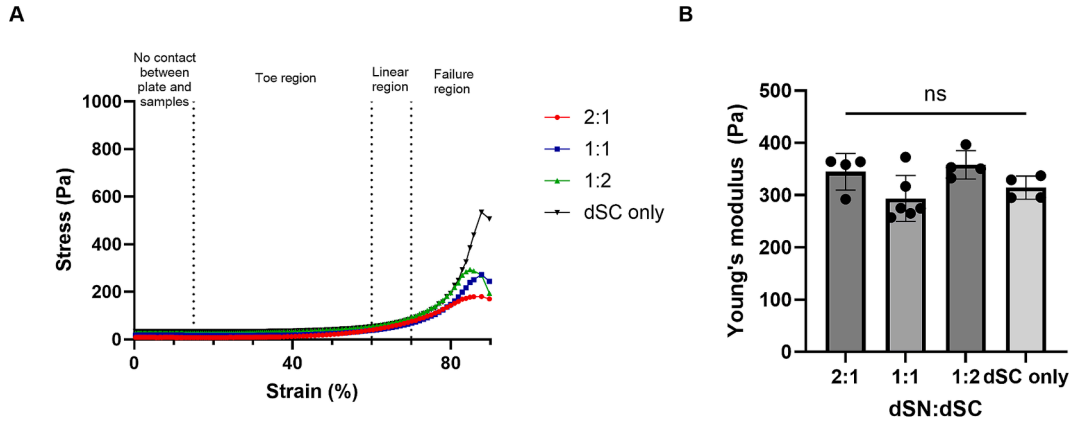

Fig. 1. Mechanical properties of composite hydrogels. A) stress–strain curves of composite hydrogels from compression test. B) Young's Modulus calculated from stress-strain curve, n = 4–6. One-way ANOVA with Tukey's multiple comparison test was performed; ns: not significant, $p > 0.05$.

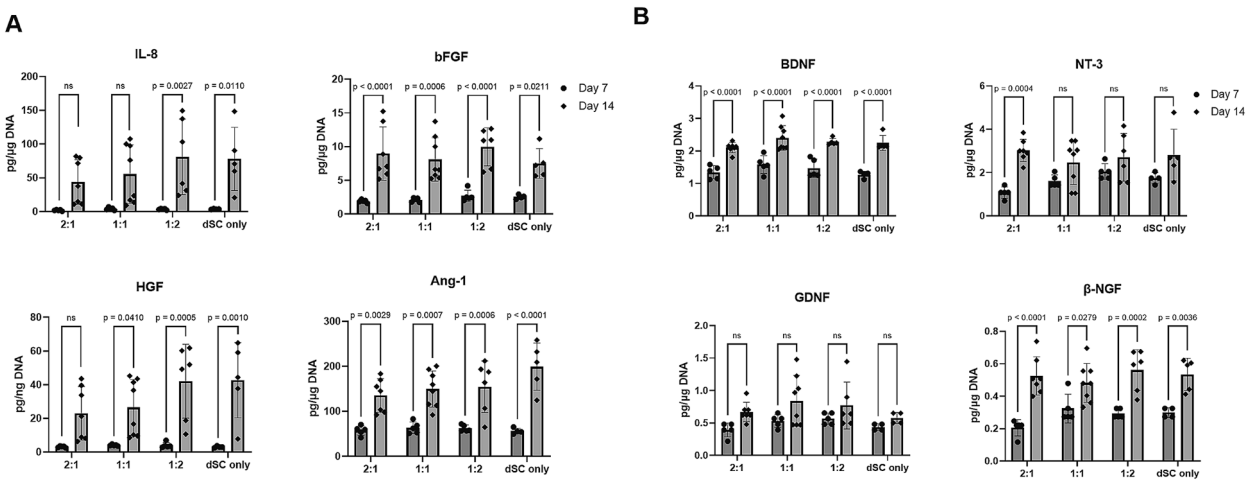

Fig. 2. Secretome analysis of hASCs-embedded nerve composite hydrogels at day 7 and day 14. A) Pro-angiogenic factors and B) neurotrophic factors, n = 4–8. A two-way ANOVA with Bonferroni multiple comparison test was performed; ns: not significant ($p > 0.05$) and p values are shown on each graph.

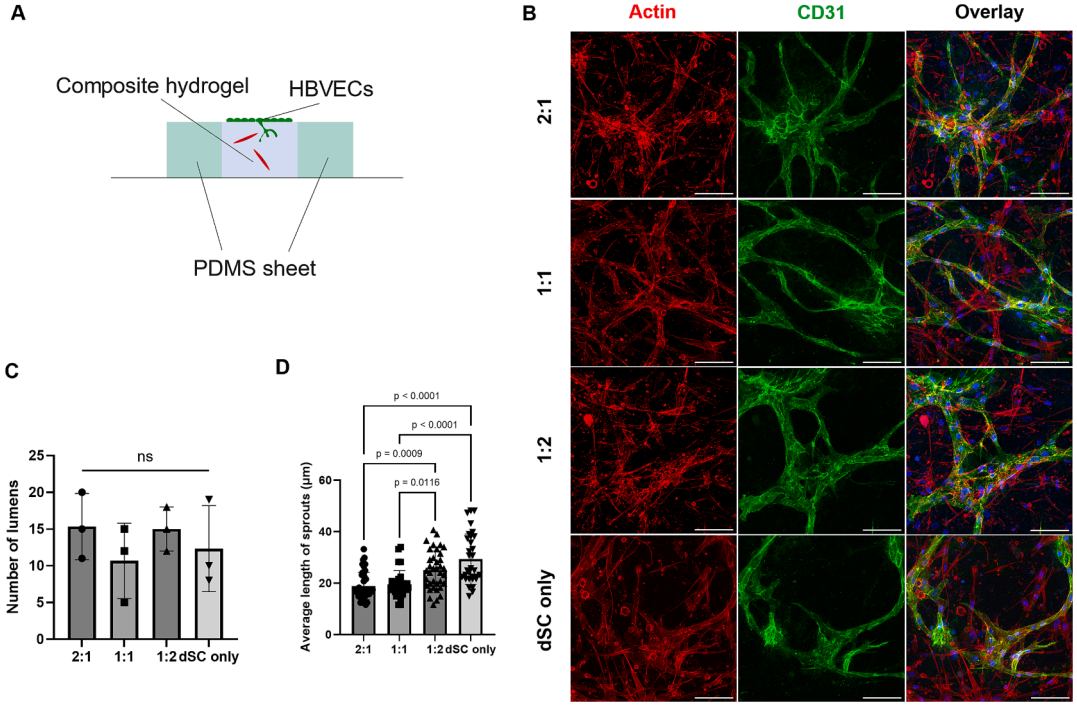

Fig. 3. HBVECs invasion assay. A) Platform for HBVECs sprouting assay to investigate pro-angiogenic effect of hASCs-embedded different ratios of composite hydrogels. B) Immunofluorescence images of composite hydrogels, F-actin (red), CD31 (green) and overlay, scale bar = 100 μm. C) Number of lumens and D) average length of sprouts that invaded the hydrogels, n = 3. One-way ANOVA with Tukey's multiple comparison test was performed; ns: not significant ($p > 0.05$) and p values are shown on each graph.

were significantly longer than those from dSN:dSC = 2:1 and 1:1 (Fig. 3D). On the other hand, HBVECs seeded after 7-day preculture of hASCs showed no or immature (not lumenized) sprouts into composite hydrogels (Supplementary Fig. S1A). A significantly higher number of endothelial lumens was observed in the dSC only hydrogel compared to the 2:1 hydrogel group (Supplementary Fig. S1B). Additionally, the average length of sprouts was significantly longer from 1:2 and dSC only hydrogel groups than those from 2:1 hydrogel group (Supplementary Fig. S1C). Upon comparing the immediate and preculture groups, a higher number of lumens and longer average length of sprouts were observed across most of the hydrogel groups (Fig. 4).

To determine whether any possible migration of hASCs towards HBVEC monolayer during the co-culture contributed to altered HBVEC sprouting between immediate and pre-culture groups, hASC presence at the top versus bulk was analyzed. Here, the bulk layer represents about 50 μm below the top hASC layer of the hydrogels. In both co-culture conditions, approximately a third of hASCs remained at the top across all hydrogel groups. Significant differences were observed in the 1:2 and dSC only hydrogel groups, with increased hASC coverage at the top of the gel after the pre-culture (Supplementary Fig. S2A). Interestingly, compared to immediate co-culture, hASC pre-culture before HBVEC introduction resulted in a significantly lower % of hASCs in the bulk of the gel across all hydrogel types (Supplementary Fig. S2B).

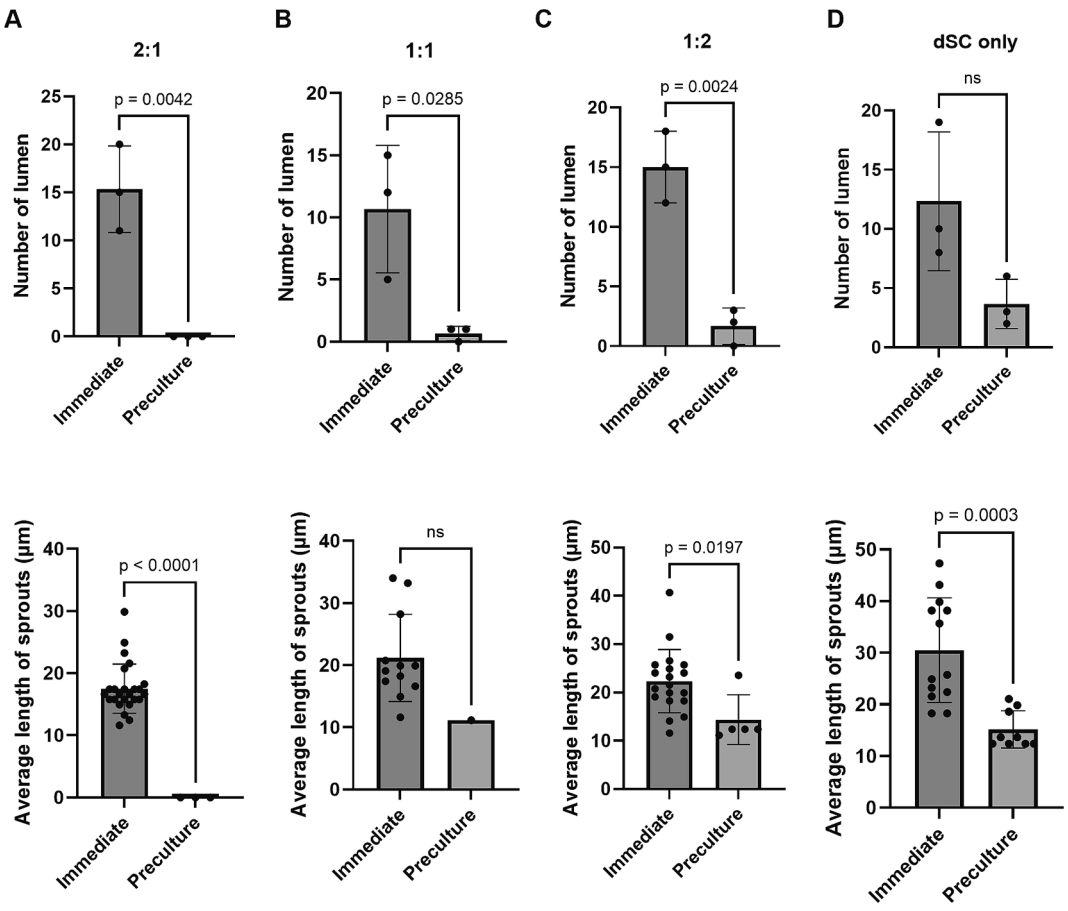

Fig. 4. Comparison of number of lumen and average length of sprouts between immediate and preculture conditions in each group; A) 2:1, B) 1:1, C) 1:2, and D) dSC only. *t*-test was performed; ns: not significant ($p > 0.05$) and p values are shown on each graph.

DRG neurite outgrowth relies on presence of hASCs or their secreted cytokines

We next assessed the effect of hASC-embedded nerve hydrogels on neurite outgrowth in vitro. DRGs were embedded into spinal cord hydrogel without ASCs and cast adjacent to composite hydrogels with ASCs either immediately or after 7 days of pre-culture and cultured for another three days in neuron media (Fig. 5A-B). In addition, to determine if the physical presence of hASCs versus hASC cytokine alone is sufficient to promote axonal regeneration, secreted factors collected after 14 days were injected into the hydrogel groups instead of hASCs.

Neurite counts were measured via Sholl analysis that provides a count of neurite intersections at different distances from the center, as we have recently demonstrated [25]. In this case, measurements were taken every 100 μm from 0 to a maximum length of neurites per image. Area under curve (AUC) of the count versus distance curve (Fig. 5C) was also calculated to quantify the extent of neurite outgrowth and compare between different ratios of hydrogels (Fig. 5D). Additionally, average longest neurites in all hydrogel groups were calculated (Fig. 5E).

When DRGs were embedded immediately, hASCs across all hydrogel groups exhibited almost no neurotrophic effect (Supplementary Fig. S3A). The number of neurites, the AUC, and the average longest neurite did not show significant differences among all hydrogel groups (Supplementary Fig. S3B-D). In contrast, multiple neurite outgrowths were observed in all 7-day preculture hydrogel groups (Fig. 5B). However, there was no significant difference of AUC and average longest neurite across these hydrogel groups (Fig. 5C-E). Similarly, DRG adjacent to the hASCs cytokine-injected composite hydrogels also showed neurite extension (Supplementary Fig. S4A), yet there was still no significant difference in neurotrophic effect among all hydrogel groups (Supplementary Fig. S4B-D).

The AUC and the average longest neurites were analyzed across three different conditions for all hydrogel groups-immediate, preculture, and injected-to determine the effect of the culture condition and physical appearance of cells on neurite outgrowth. In the dSN:dSC = 2:1 and dSC only hydrogel groups, no significant differences were observed among the conditions (Fig. 6A and 6D). However, in the 1:1 hydrogel group, both the AUC and the average longest neurites were significantly higher and longer in the preculture condition compared to the immediate condition (Fig. 6B). In the 1:2 hydrogel group, these parameters were significantly different in the preculture condition compared to immediate and injected conditions (Fig. 6C).

Proteomic profiling and analysis of fresh and decellularized SN and SC

Proteomic analysis was performed to compare and analyze ECM composition of native and decellularized sciatic nerves and spinal cords. The identified proteins were categorized into two categories with six divisions using *MatrisomeDB*: core matrisome including collagen, ECM glycoproteins, and proteoglycans, and matrisome-associated proteins including ECM-affiliated proteins, ECM regulators, and secreted factors [26].

In the context of matrisome, a total of 18 collagen, 71 ECM glycoproteins, 16 proteoglycans, 32 ECM-affiliated proteins, 62 ECM regulators, and 20 secreted factors were identified in dSN whereas a total of 20 collagen, 54 ECM glycoproteins, 18 proteoglycans, 28 ECM-affiliated proteins, 45 ECM regulators and 12 secreted factors were detected in dSC. Differences and similarities between dSN and dSC were visualized using Venn diagrams (Fig. 7A). Since matrisome-associated proteins including ECM-affiliated proteins, ECM regulators, and secreted factors

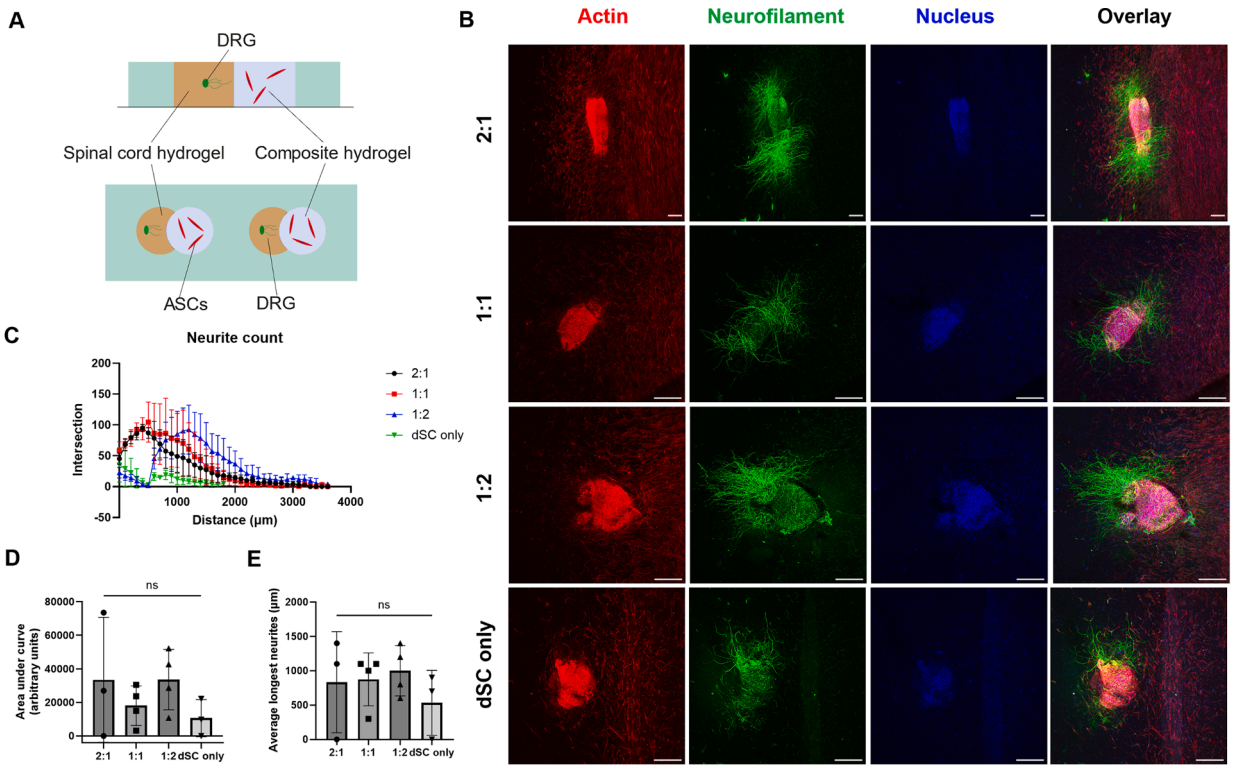

Fig. 5. Pre-culture of hASCs for 7 days prior to DRG encapsulation in dSC only hydrogel. A) Platform for DRG neurite outgrowth assay. DRG were embedded in dSC hydrogel adjacent to hASCs-embedded different ratios of composite hydrogels. B) Immunofluorescence images of composite hydrogels, F-actin (red), neurofilament (green), nucleus (blue), and overlay. C) neurite outgrowths count versus distance graph. D) The area under curve from C). D) Average longest neurites. Scale bar = 500 μm, n = 3–4. One-way ANOVA with Tukey's multiple comparison test was performed; not significant, $p > 0.05$.

are mainly proteolytic enzymes and cytokines that are not core structural ECM component, only the core matrisome; collagen, ECM glycoproteins, and proteoglycans were taken into consideration for analysis as they are essential for building the ECM structure. Some proteins, such as COL5A1, PRG4, SPARC, IGFBP7 in dSN and PODN in dSC were less observed compared to native SN and SC, however, almost all collagen family, ECM glycoproteins, and proteoglycans in both dSN and dSC showed greater expression compared to the fresh SN and SC (Fig. 7B). In Fig. 7C, the top 20 abundant ECM proteins were listed. While several ECM proteins were found to be common between dSC and dSN, their relative abundance was different. We believe this distinction may be able to highlight the tissue-specific variations in ECM composition and how they contribute to their unique functional characteristics. TNXB, COL18A1, LAMB2, HSPG2, NID1, and LAMB1 were identified as dSN-specific abundant ECM proteins while POSTN, COL1A1, COL1A2, VCAN, DPT, and CLIP2 were particularly abundant in dSC.

Ranking

To determine the best candidate for further studies, composite hydrogels were ranked based on the levels of statistical significance of experimental data discussed in this study, with 1 being the best and 4 being the worst. The final scores were calculated by summing scores from all analyses (Table 1). Taken together, dSN:dSC = 1:2 hydrogel showed the best performance in releasing pro-angiogenic and neurotrophic factors as well as supporting endothelial infiltration and neurite outgrowth in vitro. This suggests that 1:2 hydrogel may be suitable for further investigation using *in vivo* models and potential therapeutic application in SCI treatment.

Discussion

In this study, we investigated the angiogenic and neurotrophic effects of hASC-embedded nerve composite hydrogels in vitro. hASCs were encapsulated in different ratios of nerve composite hydrogels, dSN:dSC = 2:1, 1:1, 1,2 and dSC only hydrogel served as a control. dSC only hydrogel rather than dSN only hydrogel was selected as the control as the current study focused on SCI regeneration. Since the goal is to investigate how the composite hydrogels might enhance therapeutic outcomes in the context of SCI repair, dSC only hydrogel may provide the most appropriate control. By examining the secreted cytokine profiles of hASCs in different ratios of hydrogels, we were able to observe that dSN:dSC = 1:2 hydrogel group showed a significantly increased secretion of angiogenic and neurotrophic factors. Immediate introduction of HBVECs to hASC-embedded nerve composite hydrogels promoted endothelial invasion despite an increasing trend in angiogenic factors. Immediate introduction of DRG did not result in neurite outgrowth, however, precultured hASCs and injection of cytokines from hASCs within the nerve composite hydrogels promoted neurite outgrowth. We performed proteomic analysis to identify differences in ECM composition between the decellularized tissues. These differences may provide insights into why hASCs exhibit different therapeutic behavior, which warrants future investigation. Overall, our approach provides an insight into not only how different ECM components within ECM-based hydrogels may exert therapeutic effects on their own as well as onto encapsulated cells, but also targeting specific ECM proteins to improve the therapeutic efficacy of hydrogels for spinal cord injury treatment.

The stress–strain curve (Fig. 1A) exhibited the characteristics of a J-shaped exponential behavior, which is often observed in soft biomaterials such as collagen, retina and choroid [27–29]. The toe region corresponds to the initial straightening of the hydrogels and as strain

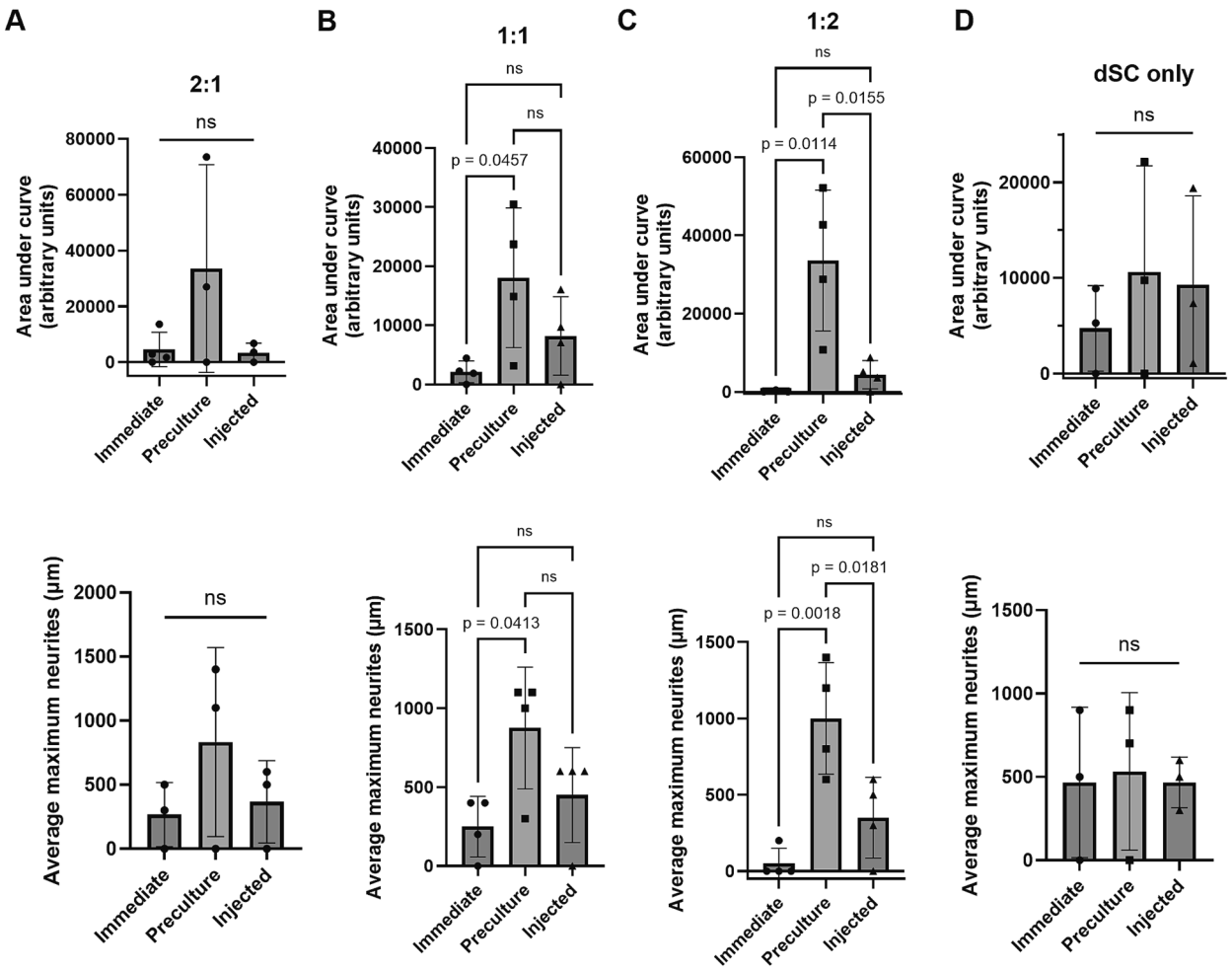

Fig. 6. Three different conditions comparative analysis-Immediate, preculture and injected-in A) 2:1, B) 1:1, C) 1:2, and D) SC only hydrogel. One-way ANOVA with Tukey's multiple comparison test was performed; ns: not significant ($p > 0.05$) and p values are shown on each graph.

increases into the elastic region, the slope becomes steeper, implying the engagement of the ECM proteins leading to a greater resistance to further compression. The curves also reached peak stresses indicating the onset of the failure of hydrogels. Calculated Young's modulus of all hydrogel groups was between 300 – 400 Pa. Soft substrates with elasticity of 0.1 – 1 kPa, similar to brain tissue, have been shown to induce mesenchymal stem cells to adopt a neuronal lineage, leading to expression of neuronal markers like β3 tubulin, neurofilament heavy chain, and its phosphorylated form, and upregulate neurogenic transcripts [30]. It is plausible that our composite hydrogels could provide an effective microenvironment to differentiate encapsulated stem cells into neurons. Further studies will confirm this hypothesis.

ASCs secrete pro-angiogenic factors such as vascular endothelial growth factor (VEGF) and angiopoietin-1 (Ang-1) that promote neovascularization, and neurotrophic factors including brain-derived neurotrophic factor (BDNF), glial-derived neurotrophic factor (GDNF), nerve growth factor (NGF), and neurotrophin-3 (NT-3) that can enhance axonal regeneration, potentially leading to improved functional recovery [8,31]. Secreted cytokines from hASCs embedded in different ratios of nerve composite hydrogels were examined to investigate the influence of ECM compositional differences on hASCs. We examined IL-8 because it regulates angiogenesis by enhancing endothelial cell survival, proliferation and matrix metalloproteinases production [32]. bFGF plays a role in mitogenesis of endothelial cells and HGF enhances angiogenesis in concert with VEGF [33,34]. Ang-1 regulates migration, adhesion, and survival of endothelial cells and also essential factor for vessel maturation [35]. The secretion level of IL-8 did not differ significantly between day 7 and day 14 from dSN:dSC = 2:1 and 1:1 hydrogel group. In contrast, HGF was released markedly higher on day 14 compared to day 7 in 1:1, 1:2, and dSC only hydrogels. Notably, 1:2 and dSC only hydrogel groups exhibited increased secretion of all angiogenic factors on day 14. Next, neurotrophic factors were investigated; NT-3, BDNF, GDNF, and β-NGF. NT-3 facilitate not only survival, proliferation, and differentiation of neuron, but also promotes axonal regeneration after injury [36,37]. BDNF is one of the widely investigated neurotrophic factors and it enhances neurite growth, neural regeneration, and functional recovery [38,39]. GDNF also exhibits a survival effect on various neurons within the CNS and plays multiple other roles in regulating nervous system functions [40]. β-NGF is considered an important mediator of neuronal survival, development, function and axonal growth [41,42]. Neurotrophin analysis showed similar trends as angiogenic factor results, increased secretion across all hydrogel groups at day 14 compared to day 7. While the precise mechanism of increased cytokine secretions over time remains unclear and was not investigated in the current study, it is possible that changes in cell signaling pathways, interactions with the surrounding microenvironments, and gene expression over time attribute to the increased growth factor release. Future studies should aim to explore these mechanisms to provide deeper insights into how to optimize conditions for improved therapeutic potentials and eventually functional recovery.

Our secreted cytokine profile highlights the importance of hydrogel composition in modulating hASCs behavior and cytokines release over time. Interestingly, dSN:dSC = 1:2 hydrogel demonstrated a significant increase in secretion of almost all analytes by encapsulated hASCs at day

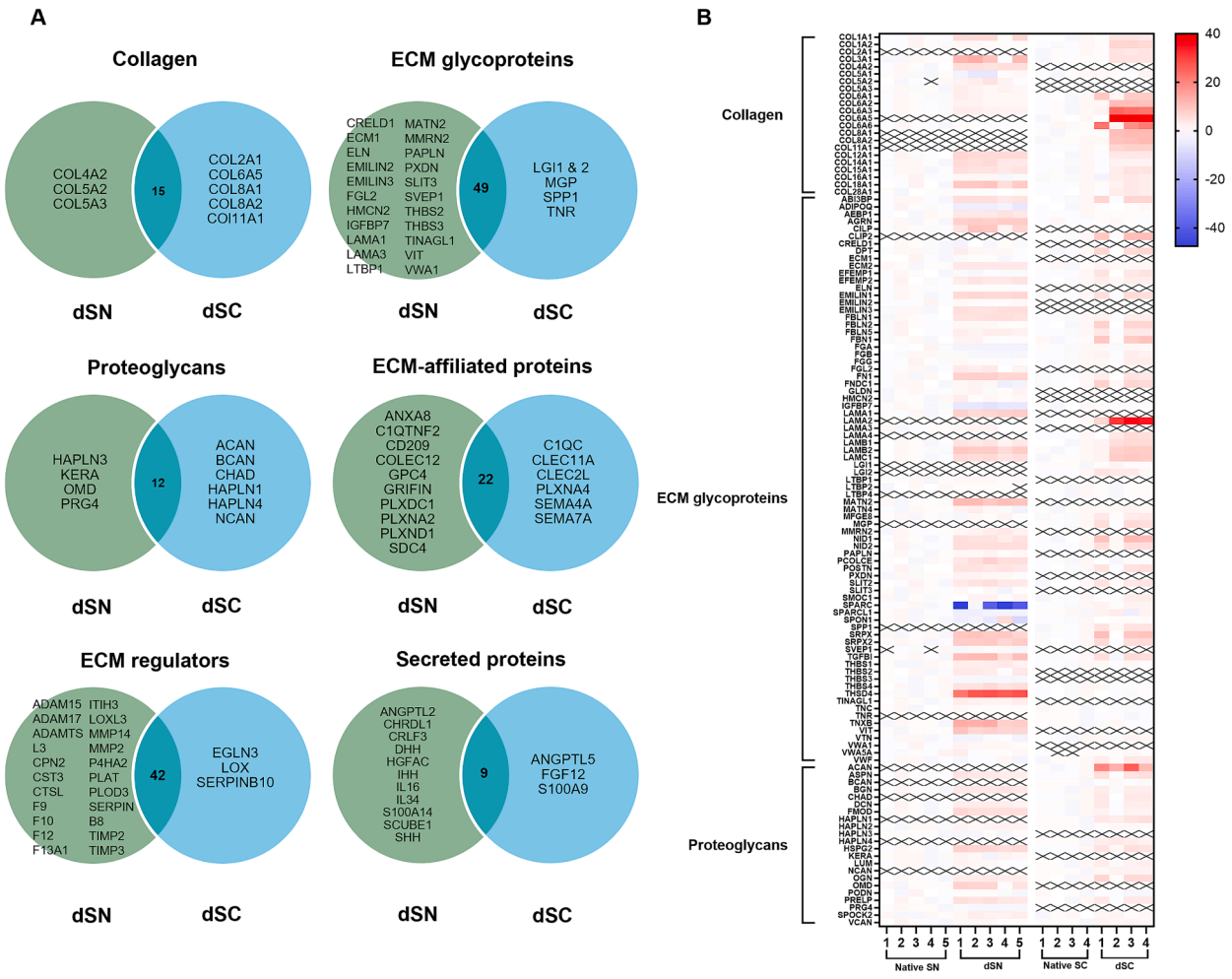

C

	Decellularized sciatic nerve		Decellularized spinal cord	
Rank	Gene symbol	Description	Gene symbol	Description
1	COL14A1	Collagen type XIV alpha 1 chain	OGN	Mimecan
2	PRELP	Prolargin	COL12A1	Collagen type XII alpha 1 chain
3	OGN	Mimecan	COL6A2	Collagen type VI alpha 2 chain
4	DCN	Decorin	PRELP	Prolargin
5	LUM	Lumican	COL6A1	Collagen type VI alpha 1 chain
6	COL12A1	Collagen type XII alpha 1 chain	COL6A3	Collagen type VI alpha 3 chain
7	COL6A2	Collagen type VI alpha 2 chain	TGFBI	Transforming growth factor-beta-induced protein ig-h3
8	**TNXB**	**Tenascin XB**	**POSTN**	**Periostin**
9	LAMC1	Laminin subunit gamma 1	**COL1A1**	**Collagen type I alpha 1 chain**
10	COL6A1	Collagen type VI alpha 1 chain	COL14A1	Collagen type XIV alpha 1 chain
11	**COL18A1**	**Collagen type XVIII alpha 1 chain**	LUM	Lumican
12	BGN	Biglycan	**COL1A2**	**Collagen type I alpha 2 chain**
13	**LAMB2**	**Laminin subunit beta 2**	BGN	Biglycan
14	ASPN	Asporin	DCN	Decorin
15	**HSPG2**	**Heparan sulfate proteoglycan 2**	ABI3BP	Target of Nesh-SH3
16	ABI3BP	Target of Nesh-SH3	**VCAN**	**Versican**
17	**NID1**	**Nidogen 1**	**DPT**	**Dermatopontin**
18	TGFBI	Transforming growth factor-beta-induced protein ig-h3	**CLIP2**	**Cartilage intermediate layer protein 2**
19	COL6A3	Collagen type VI alpha 3 chain	LAMC1	Laminin subunit gamma 1
20	**LAMB1**	**Laminin subunit beta 1**	ASPN	Asporin

Fig. 7. Proteomic analysis on fresh and decellularized sciatic nerve and spinal cord (n = 4/5). A) Venn diagrams showing the differences between dSN and dSC at six different divisions; collagens, ECM glycoproteins, proteoglycans, ECM-regulators, ECM-affiliated proteins, and secreted factors. B) Heatmap of collagen, ECM glycoproteins, and proteoglycans identified from proteomics. C) Top 20 abundant proteins in dSN and dSC, sorted by their log2VSN (variance stabilizing normalization), color-coded; collagens (blue), ECM glycoproteins (orange), and proteoglycans (green) and tissue-specific abundant proteins are highlighted in bold.

14 compared to day 7. The enhanced and prolonged secretion from the 1:2 hydrogel suggested that this specific composition of the hydrogels can provide a more favorable microenvironment for encapsulated hASCs. It may be able to address the limitation of direct administration of growth factors at the site of injury since they can be rapidly cleared and/or degraded and eventually reduce therapeutic efficacy [25].

Angiogenic response by HBVECs to hASC-embedded composite hydrogels seems to have depended on the co-culture condition and hASC

Table 1
Ranking of different hydrogel groups based on analysis of hASC cytokines and co-culture studies. Hydrogel groups were ranked from 1 to 4 (1 being the best, 4 being the worst) for each parameter listed below.

	Hydrogel Ratio			
Analysis Parameter	2:1	1:1	1:2	dSC only
IL-8	3	3	1	2
HGF	4	3	1	1
bFGF	1	3	1	4
Angiopoietin-1	4	2	2	1
NT-3	1	2	2	2
β-NGF	1	4	2	3
BDNF	1	1	1	1
GDNF	1	1	1	1
HBVEC sprouting	3	3	1	1
DRG neurite infiltration	1	1	1	1
Final score	**20**	**23**	**13**	**17**

location throughout the gel. When HBVECs were seeded immediately, endothelial sprouts were formed across all hydrogel groups while no or immature sprouts were observed following hASC pre-culture in all hydrogel groups. This result may indicate that pro-angiogenic effect of our combinatorial therapeutic may occur during the earlier periods of co-culture. Another possible reason behind decreased endothelial sprouting after hASC pre-culture is increased presence of hASCs at the top layer interfacing HBVEC monolayer. This top layer of hASCs may have acted as a physical barrier that inhibited endothelial infiltration into the hydrogels. Interestingly, our result contrasts with findings from another study that reported increased endothelial sprouting when endothelial cells were seeded atop hASC-laden collagen hydrogels following 7 days of pre-culture [43]. In this study, increased presence of hASCs at the top was found after immediate co-culture. This discrepancy may be attributed to differences in experiment conditions, such as hydrogel types (nerve composite versus type I collagen), endothelial cell types used [HBVECs versus human umbilical vein endothelial cells (HUVECs)], etc. While in the previous study HUVECs deposited basement membrane during immediate co-culture, our combinatorial platform already contains basement membrane components. It is possible that this difference in ECM milieu triggered overlaid HBVECs to respond favorably to pro-angiogenic cues from embedded hASCs early on. In our studies, a similar number of endothelial lumens were formed across hydrogel groups, however, longer sprouts were formed in the 1:2 hydrogels. With this result, we also postulate that the ECM compositional difference across our hydrogel groups may also affect pro-angiogenic capacity of hASC-embedded nerve composite hydrogels.

For the DRG neurite outgrowth assay, DRG were embedded in a separate spinal cord hydrogel adjacent to the different ratios of nerve composite hydrogels to recapitulate a site of injury as shown in Fig. 5A. DRG-embedded spinal cord hydrogel was designed to mimic an endogenous microenvironment, while hASC-laden nerve composite hydrogels represent therapeutic administration at the injury site. In this platform, we observed a lack of neurite outgrowth in the immediate co-culture condition across all hydrogel groups; however, in a preculture condition, we were able to observe axons extending from the overlaid DRGs. It is possible that an immediate introduction of nerve composite hydrogels did not provide a conducive environment for neurite extension because there was not sufficient time for axons to interact with ECM components within the hydrogels and cytokines from hASCs. In contrast, the preculture period presumably allowed axons to communicate with ECM and growth factors secreted from hASCs that might contribute to a favorable environment for neurite outgrowth. Across the three culture conditions, no significant difference was found between all hydrogel groups, indicating that our ECM compositional differences have little effect on neurite outgrowth.

Comparative analysis on three different DRG embedded conditions highlighted the role of culture condition and cellular presence on neurite outgrowth within the hydrogels. There were no significant differences in the AUC and the average longest neurites in the dSN:dSC = 2:1 and dSC only hydrogel groups, suggesting that these compositions provide an environment irrespective of the culture conditions. However, the significant differences in the AUC and the average longest neurites in the 1:1 and 1:2 groups underscore the importance of culture condition. The significant difference between preculture and injected condition in 1:2 group indicated that cellular presence might influence neurite extension due to prolonged secretion of growth factors and injected cytokines might have degraded or diffused rapidly in this composition. The same trend across all hydrogel groups was noted, higher AUC and longer average longest neurites in preculture condition compared to immediate and injected conditions. These results are consistent with our neurotrophic factors secretion results, showing an increased secretion of neurotrophic factors over time. Enhanced neurite outgrowth and longer neurites are likely affected by the amount of secreted factors.

It is worth noting that while our co-culture studies were performed either immediately or after seven days of hASC preculture, co-culture responses after 14 days of preculture were not assessed. We assessed immediate or 7-day preculture responses to focus on the early effect of our therapeutic. This early assessment might reveal critical insights into the early signs of angiogenesis and axonal regeneration and provide an understanding of how cells interact with the hydrogels during the early phases of wound healing. To better correlate our Luminex data to HBVEC and DRG responses, future studies will also need to determine 14-day preculture effects for more comprehensive evaluation of long-term cellular responses therapeutic potentials. More angiogenic and neurotrophic factors were observed after the 14-day preculture, however, it may not lead to promoted neovascularization and axon regeneration as mentioned above. Additional investigation of MMPs ECM-degrading activity and degradation pores as previously demonstrated to contribute to endothelial sprouting [43] will be necessary to confirm these conclusions. The effects of preculture are also intriguing since it had a negative effect on angiogenic potential and a positive effect on the DRG neurite outgrowth. As mentioned earlier, increased migration of ASCs to the top of the hydrogels during pre-culture may have resulted in reduced endothelial sprouting. However, it may be resolved by optimizing cell encapsulation density for HBVECs infiltration assay as cell density within the hydrogels can significantly influence cell behavior and experimental outcome in 3D culture [44]. In addition, the effects of pre-culture might be due to a possible shift in the secretory behavior of the hASCs from day 0 to day 7. Angiogenic and neurotrophic factor analyses between days 0 and 7 may help to understand this behavior. Also, RNA-seq transcriptomic profiling could provide insights on gene expression changes at the early time point.

Proteomic analysis provided us with a comprehensive profile of proteins contained in native and decellularized tissues. We were able to categorize them into six different divisions and found out there are several dSN- and dSC-specific proteins that might affect hASCs behaviors. Given the complexity and the extensive list of proteins identified in the proteomics data, we focused our analysis on the top 20 most abundant ECM components to simplify the results. It was expected to provide a clear understanding of the functional contributions of these ECM components to hASCs behaviors.

The collagen division identified 15 overlaps, three dSN-specific and five dSC-specific collagens. COL4A2 was one of the dSN-specific collagen and type IV collagen is known to be a main component of basement membrane. Preexisted COL4A2 in dSN could serve as a part of basement membrane that might prevent endothelial sprouting. COL18A1 is neither dSN- nor dSC-specific protein, however, it is one of the top 20 abundant proteins found in dSN. Type XVIII collagen and its carboxyl-terminal fragment, endostatin, are known to have anti-angiogenic activity in vitro and *in vivo* [45]. In addition, COL8A1 and COL8A2 were found only in dSC. Type VIII collagen is reported to play a role in angiogenesis and vascular remodeling [46,47].

As for ECM glycoproteins, 49 common proteins were found between

dSN and dSC and 22 proteins were only observed in dSN. THBS2, a dSN-specific protein, can inhibit angiogenesis by preventing endothelial cell proliferation and inducing apoptosis, However, it plays a role in synapse formation and axonal sprouting [48,49]. Tenascin-R (TNR), dSC-specific protein in our study, is a glycoprotein predominantly expressed in the CNS and it is involved in regulating neurogenesis [50]. Periostin (POSTN), which is one of the top 20 abundant proteins in dSC, is known to promote neurite extension through activation of focal adhesion kinase (FAK) and AKT signaling pathways, which is crucial for cellular survival and growth mechanism [51].

The proteoglycan division identified 13 common proteins, three and five dSN- and dSC-specific proteins, respectively. ChABC was utilized during SN decellularization to remove proteoglycans, however, prolargin (PRELP), mimecan (OGN), and lumican (LUM) are the most abundant proteins in dSN. It is because PRELP, OGN, and LUM are classified as small leucin-rich proteoglycans (SLRP) that contain few glycosaminoglycan (GAG) chains that ChABC targets [52]. Therefore, these SLRPs are unlikely to be affected by ChABC. There was no ChABC step during SC decellularization, and it may explain why Aggrecan (ACAN), brevican (BCAN), and neurocan (NCAN) were only found in dSC. Proteoglycans are widely known as the main inhibitors for CNS regeneration. Thus, additional enzymes to degrade SLRP or keratan sulfate (KS) during decellularization steps may enhance neurite extension.

It is noteworthy that tissue inhibitors of metalloproteinases-2 and 3 (TIMP2 and 3) were detected in dSN even though they are not core matrisome we analyzed since they are reported to inhibit endothelial cell invasion [53]. Based on this finding, it can be inferred that hydrogels with a lower proportion of dSN and a higher proportion of dSC may provide a favorable environment for angiogenesis and vascular remodeling. While this conjecture needs to be validated, our results demonstrated that 1:2 hydrogel significantly promoted the formation of longer endothelial sprouts.

There are limitations of the current study that can be addressed in the future. First and foremost, it is essential to dive into the molecular mechanisms underlying the interactions between different ECM compositions and encapsulated hASCs. Future studies should aim to investigate the pathways and signaling molecules involved in promoting angiogenic and neurotrophic effects. Additionally, elucidating the effect of ECM composition on gene expression and protein synthesis on embedded cells may provide valuable insights on how the surrounding microenvironment influences cells behavior. In addition, one of the main disadvantages of decellularization is batch-to-batch inconsistency, however, controlled utilization of same type of animals, such as age, gender, weight, and diet may help mitigate this challenge [24]. In this study, 3-week-old rats were utilized for DRG study, however, newborn or neonatal rats DRG are also widely used due to their higher growth and regenerative capacity [25]. DRG from younger rats may yield better neurite extension. Finally, while our DRG studies showed promising results of our combinatorial platform, further investigation should include directionality of neurite outgrowth. If we can guide regenerating axons, it would improve the accuracy and efficiency of regenerating the axons at the injury site, potentially leading to better functional recovery.

In conclusion, we have demonstrated the therapeutic potentials, especially angiogenic and neurotrophic effects of hASCs-laden nerve composite hydrogels. Particularly, dSN:dSC = 1:2 hydrogel was shown to be the most effective composition for inducing angiogenesis and axonogenesis based on our findings and will be the focus of future investigations in the context of SCI repair. Collectively, this research sheds light on not only the significance of culture conditions and ECM compositional differences in promoting regenerative potential but also the development of effective combinatorial therapy for better functional restoration.

Materials and methods

Cell culture

Human ASCs and human brain microvascular endothelial cells (HBVECs) were purchased from Lonza and Cell System, respectively. Human ASCs of passage 2 through 5 were cultured in growth media (ADSC-GM, Lonza) and HBVECs of passage 4 through 8 were cultured in growth media (EGM2-MV, Lonza). Cells were maintained at 37 °C, 5 % CO_2 and media were changed every 2 days.

ECM hydrogel production

Porcine spinal cords (SC) and sciatic nerves (SN) were purchased from Tissue Sources LLC. The tissues were frozen at −80 °C upon delivery, thawed immediately prior to use, and then decellularized according to the tissue-specific methods as previously described [24]. Chemicals used in the process were purchased from Millipore Sigma unless stated otherwise. Briefly, spinal cords were rinsed in water, trypsin (Thermo Fisher), Triton X-100, sucrose, deoxycholic acid, DNase, phosphate buffered saline (PBS, VWR), and peracetic acid (Lab Alley). Sciatic nerves were washed in water, salt buffers, SB-10, SB-16, Chondroitinase ABC (ChABC), and DNase. All steps except DNase and ChABC incubations were performed under orbital agitation. After decellularization, tissues were lyophilized and separately digested in a 0.01 N HCl solution containing 1 mg/ml pepsin at a tissue concentration of 15 mg/ml and stirred at 4 °C temperature for 72 h to form pre-gel solutions. Composite hydrogels were made by mixing dSN and dSC pre-gel solutions at following ratios between dSN:dSC = 2:1, 1:1, and 1:2. dSC only hydrogel was utilized as a control in all experiments.

Polydimethylsiloxane (PDMS) microwell fabrication and 3D culture

PDMS microwells were fabricated via soft photolithography as previously described [24]. Briefly, Si wafer was etched with a SU-8 photoresist to generate circular patterns of 200 μm in depth and 4 mm in diameter. PDMS base and curing agent were mixed at a ratio of 10:1, poured onto the Si wafer, and cured for 2 h at 60 °C. The cured PDMS sheet was demolded and punched out using an 8 mm diameter biopsy punch. Microwells were air plasma treated (Harrick Plasma) and functionalized with 1 % [v/v] polyethyleneimine (PEI, Sigma) and 0.1 % [v/v] glutaraldehyde (GA, Sigma). Different ratios of composite pre-gel solutions were cast with ASCs embedded at 1 million cells/ml.

Proteomic analysis – CME methods (Orbitrap Exploris DIA)

Total protein from each tissue sample was reduced, alkylated, and purified by chloroform/methanol extraction prior to digestion with sequencing grade modified porcine trypsin (Promega). Tryptic peptides were then separated by reverse phase XSelect CSH C18 2.5 um resin (Waters) on an in-line 150 x 0.075 mm column using an UltiMate 3000 RSLCnano system (Thermo). Peptides were eluted using a 60 min gradient from 98:2 to 65:35 buffer A:B ratio. Eluted peptides were ionized by electrospray (2.2 kV) followed by mass spectrometric analysis on an Orbitrap Exploris 480 mass spectrometer (Thermo). To assemble a chromatogram library, six gas-phase fractions were acquired on the Orbitrap Exploris with 4 *m/z* DIA spectra (4 *m/z* precursor isolation windows at 30,000 resolution, normalized AGC target 100 %, maximum inject time 66 ms) using a staggered window pattern from narrow mass ranges using optimized window placements. Precursor spectra were acquired after each DIA duty cycle, spanning the *m/z* range of the gas-phase fraction (i.e. 496–602 *m/z*, 60,000 resolution, normalized AGC target 100 %, maximum injection time 50 ms). For wide-window acquisitions, the Orbitrap Exploris was configured to acquire a precursor scan (385–1015 *m/z*, 60,000 resolution, normalized AGC target 100 %, maximum injection time 50 ms) followed by 50x 12

m/z DIA spectra (12 *m/z* precursor isolation windows at 15,000 resolution, normalized AGC target 100 %, maximum injection time 33 ms) using a staggered window pattern with optimized window placements. Precursor spectra were acquired after each DIA duty cycle.

Buffer A = 0.1 % formic acid, 0.5 % acetonitrile

Buffer B = 0.1 % formic acid, 99.9 % acetonitrile

Following data acquisition, data were searched using an empirically corrected library against the UniProt *Sus scrofa* database (January 2022) and a quantitative analysis was performed to obtain a comprehensive proteomic profile. Proteins were identified and quantified using EncyclopeDIA [54] and visualized with Scaffold DIA using 1 % false discovery thresholds at both the protein and peptide level. Protein MS2 exclusive intensity values were assessed for quality using ProteiNorm [55]. The data was normalized using VSN [56] and analyzed using proteoDA to perform statistical analysis using Linear Models for Microarray Data [57] with empirical Bayes (eBayes) smoothing to the standard errors. Proteins with an FDR adjusted p-value < 0.05 and a fold change > 2 were considered significant.

Compression test

The compression test was conducted using a rheometer (DHR 2, TA Instruments) to analyze the mechanical property of the hydrogels. Hydrogels were fabricated in a PDMS mold with a diameter of 8 mm and a height of 2–3 mm, with a volume of 100 μl. Hydrogels were compressed with a load of 250 N in between 40 mm diameter stainless-steel parallel plates. All tests were performed at a rate of 10 % of height until failure at room temperature. The data were collected as strain (%) versus strain curve (Pa). Parallel plates started compressing approximately 1 mm above of the hydrogels, therefore, initial ~15 % of the curve was not considered as a data point. Young's modulus was calculated from the slope of the linear region of the curve.

Analysis of pro-angiogenic and neurotrophic factor secretion

After 7- and 14-day of culture, serum-free media was added and collected after 24 h in culture. Collected media were concentrated 5-fold through 3 kDa MWCO concentration filter centrifugal tubes (Millipore). Human Premixed Multi-Analyte Kits (Magnetic Luminex Assay, R&D Systems) were used to analyze multiple cytokines, including pro-angiogenic factors; interleukin-8 (IL-8), basic fibroblast growth factor (bFGF), hepatocyte growth factors (HGF), angiopoietin-1 (Ang-1), and neurotrophins; nerve growth factor (NGF), neurotrophin-3 (NT-3), glial cell-derived neurotrophic factor (GDNF), and brain-derived neurotrophic factor (BDNF). All reagents were prepared according to the manufacturer's instructions. Results were normalized to dsDNA content. The amount of dsDNA was quantified using DNeasy Blood and Tissue Kit (Qiagen).

HBVECs invasion assay

For HBVECs invasion assay, composite hydrogels were cast either in microwells or PDMS strip that was cut and placed on glass coverslip. After gelation at 37 °C, hydrogels in microwells or PDMS strip were overlaid with HBVECs at a density of 471,000 cells/ml either immediately or after 7-day pre-culture of ASCs to ensure confluent endothelial monolayer formation. Pre-culture was performed in ADSC-GM and invasion assay was performed in invasion media consisting of HBVEC growth media supplemented with 50 μg/ml L-ascorbic acid (Acros Organics) and 50 ng/ml tetradecanoyl phorbol acetate (TPA, Cell Signaling Technology) for 7 days as previously described [58]. ImageJ was used to analyze endothelial sprouting analysis. Endothelial sprouts less than 10 μm in length were not included in the analysis [43]. A number of endothelial lumens was counted manually at the surface of hydrogels. The length of endothelial sprouts was determined by measuring the number of stacks the sprouts penetrated from the surface through the hydrogels. hASC percentage area was analyzed by creating top and bulk images using Z-stack maximum intensity projection, with the top layer representing the hASC layer, 0–25 μm on average, and the bulk layer representing an average of 50 μm below hASC layer, followed by analyzing the percentage area using ImageJ.

DRG harvest, coculture and neurite outgrowth quantification

The animal studies were approved by the Institutional Animal Care and Use Committee (IACUC) of the University of Arkansas (protocol numbers: 20054 and 23019). Male Sprague Dawley rats between 3–4 weeks old and 35–49 g were ordered from Envigo and euthanized using CO_2 asphyxiation.

Rat DRGs were harvested as previously described [59]. Briefly, the hemi-segment of spinal column was generated after transverse and sagittal cut of spinal cord. The DRGs were visualized by dissection microscope (Leica), removed carefully with forceps, trimmed, and collected in Ham's F12 media on ice until use on the same day.

Custom-made PDMS sheets were punched out using an 8 mm biopsy punch to make PDMS strips with complete and truncated circular patterns. PDMS strips were placed on glass slips, plasma cleaned, and PEI and GA treated as described. Composite hydrogel with hASCs were cast in the complete circular pattern, and DRG were embedded in dSC only hydrogel in the truncated circular pattern either immediately or after preculture of 7 days. Following the incubation, neuron media was added to the hydrogels and incubated for another 3 days. In addition, collected cytokines were injected into the dSC only hydrogel that DRGs were embedded to determine if hASC cytokines alone can induce neurite outgrowth. Sholl analysis toll in the SNT plugin in Fiji was utilized to quantify the DRG neurite outgrowth as previously reported [25]. Stacked images were projected with maximum intensity, intersections in each shell were counted with an interval of 100 μm.

Immunofluorescence and confocal imaging

All hydrogel groups were fixed in 4 % formaldehyde, washed with PBS, permeabilized with 0.05 % Triton-X (VWR) in PBS, and blocked with bovine serum albumin (BSA, Fisher Scientific). The samples were incubated with primary antibodies at 4 °C overnight. Primary antibodies used in this study are mouse anti-CD31 (1:200, Abcam, ab9498) and mouse anti-neurofilament (1:500, Developmental Studies hybridoma Bank, RT97). After rinsing with 0.05 % Tween-20 in PBS, the samples were incubated with secondary antibodies (goat anti-mouse Alexa Flour® 488; goat anti-rabbit Alexa Fluor® 647). Cell nuclei and cytoskeleton were stained with DAPI and Alexa Fluor® phalloidin 568, respectively. Confocal images were acquired using Olympus IX83 confocal microscope. Images of 4 at the center of hydrogels were taken with 20X magnification. To visualize neurite outgrowth and endothelial cell invasion, ImageJ was used to compile stacks into a maximum intensity projection.

Statistical analysis

Statistical analysis was performed in GraphPad Prism 9.5.1 using student's *t*-test, one- and two-way analysis of variance (ANOVA) followed by Tukey's and Bonferroni's post-hoc test for multiple pairwise comparisons. Outliers were eliminated using Grubbs test. All data are presented as mean ± standard deviation.

CRediT authorship contribution statement

Inha Baek: Writing – review & editing, Writing – original draft, Visualization, Validation, Methodology, Investigation, Formal analysis, Data curation. **Younghye Song:** Writing – review & editing, Supervision, Project administration, Methodology, Funding acquisition, Conceptualization.

Declaration of competing interest

The authors declare that they have no known competing financial interests or personal relationships that could have appeared to influence the work reported in this paper.

Acknowledgements

This work was supported by PhRMA foundation and the National Institutes of Health through the award numbers P20GM139768, R15NS121884 and R37CA279722 awarded to YS as well as R24GM137786 to the IDeA National Resource for Quantitative Proteomics Core. We want to thank Dr. Kartik Balachandran and Dr. Raj Rao for letting us use their equipment. Also, we want to thank Dr. Jorge Almodovar and Dr. Luis Pinzon-Herrera for providing training on Luminex. In addition, we want to thank the University of Arkansas for Medical Sciences Proteomics Facility for mass spectrometry support. Finally, we want to thank all the undergraduate students in Song lab for helping with decellularization of porcine spinal cords and sciatic nerves.

Appendix A. Supplementary data

Supplementary data to this article can be found online at https://doi.org/10.1016/j.mbplus.2024.100165.

Data availability

Data will be made available on request.

References

[1] J. Hu, J. Shangguan, P. Askar, J. Xu, H. Sun, S. Zhou, C. Zhu, W. Su, Y. Gu, Decellularization alters the unfavorable regenerative adverse microenvironment of the injured spinal cord to support neurite outgrowth, Annals of Translational Medicine 10 (2022) 934, https://doi.org/10.21037/atm-22-3969.

[2] T. Führmann, P.N. Anandakumaran, M.S. Shoichet, Combinatorial therapies after spinal cord injury: how can biomaterials help? Advanced Healthcare Materials 6 (2017) 1–21, https://doi.org/10.1002/adhm.201601130.

[3] J.W. Rowland, G.W.J. Hawryluk, B. Kwon, M.G. Fehlings, Current status of acute spinal cord injury pathophysiology and emerging therapies: promise on the horizon, Neurosurgical Focus 25 (2008) 1–3, https://doi.org/10.3171/FOC.2008.25.11.E2.

[4] B. Fan, Z. Wei, X. Yao, G. Shi, X. Cheng, X. Zhou, H. Zhou, G. Ning, X. Kong, S. Feng, Microenvironment imbalance of spinal cord injury, Cell Transplantation 27 (2018) 853–866, https://doi.org/10.1177/0963689718755778.

[5] L.E. Kokai, K. Marra, J.P. Rubin, Adipose stem cells: biology and clinical applications for tissue repair and regeneration, Translational Research 163 (2014) 399–408, https://doi.org/10.1016/j.trsl.2013.11.009.

[6] L. Gao, Y. Peng, W. Xu, P. He, T. Li, X. Lu, G. Chen, Progress in stem cell therapy for spinal cord injury, Stem Cells International 2020 (2020), https://doi.org/10.1155/2020/2853650.

[7] P. Pagella, S. Miran, E. Neto, I. Martin, M. Lamghari, T.A. Mitsiadis, Human dental pulp stem cells exhibit enhanced properties in comparison to human bone marrow stem cells on neurites outgrowth, The FASEB Journal (2020) 1–13, https://doi.org/10.1096/fj.201902482R.

[8] P.J. Kingham, M.K. Kolar, L.N. Novikova, L.N. Novikov, M. Wiberg, Stimulating the neurotrophic and angiogenic properties of human adipose-derived stem cells enhances nerve repair, Stem Cells and Development 23 (2014) 741–754, https://doi.org/10.1089/scd.2013.0396.

[9] M. Bydon, W. Qu, F.M. Moinuddin, C.L. Hunt, K.L. Garlanger, R.K. Reeves, A. J. Windebank, K.D. Zhao, R. Jarrah, B.C. Trammell, S. El Sammak, G. D. Michalopoulos, K. Katsos, S.P. Graepel, K.L. Seidel-Miller, L.A. Beck, R. S. Laughlin, A.B. Dietz, Intrathecal delivery of adipose-derived mesenchymal stem cells in traumatic spinal cord injury: Phase I trial, Nature Communications 15 (2024), https://doi.org/10.1038/s41467-024-46259-y.

[10] Y. Shimizu, E.H. Ntege, E. Takahara, N. Matsuura, R. Matsuura, K. Kamizato, Y. Inoue, Y. Sowa, H. Sunami, Adipose-derived stem cell therapy for spinal cord injuries: advances, challenges, and future directions, Regenerative Therapy 26 (2024) 508–519, https://doi.org/10.1016/j.reth.2024.07.007.

[11] R.C. Assunção-Silva, E.D. Gomes, N. Sousa, N.A. Silva, A.J. Salgado, Hydrogels and cell based therapies in spinal cord injury regeneration, Stem Cells International 2015 (2015), https://doi.org/10.1155/2015/948040.

[12] D. Cai, W. Weng, Development potential of extracellular matrix hydrogels as hemostatic materials, Frontiers in Bioengineering and Biotechnology 11 (2023) 1–15, https://doi.org/10.3389/fbioe.2023.1187474.

[13] R.J. Muckom, R.G. Sampayo, H.J. Johnson, D.V. Schaffer, Advanced materials to enhance central nervous system tissue modeling and cell therapy, Advanced Functional Materials 30 (2020) 1–24, https://doi.org/10.1002/adfm.202002931.

[14] K.V. Nguyen-Ngoc, K.J. Cheung, A. Brenot, E.R. Shamir, R.S. Gray, W.C. Hines, P. Yaswen, Z. Werb, A.J. Ewald, ECM microenvironment regulates collective migration and local dissemination in normal and malignant mammary epithelium, Proceedings of the National Academy of Sciences of the United States of America 109 (2012) 19–24, https://doi.org/10.1073/pnas.1212834109.

[15] E.W. Raines, The extracellular matrix can regulate vascular cell migration, proliferation, and survival: relationships to vascular disease, International Journal of Experimental Pathology 81 (2000) 173–182, https://doi.org/10.1046/j.1365-2613.2000.00155.x.

[16] H. Bi, L. Ming, R. Cheng, H. Luo, Y. Zhang, Y. Jin, Liver extracellular matrix promotes BM-MSCs hepatic differentiation and reversal of liver fibrosis through activation of integrin pathway, Journal of Tissue Engineering and Regenerative Medicine 11 (2017) 2685–2698, https://doi.org/10.1002/term.2161.

[17] C.J. Medberry, P.M. Crapo, B.F. Siu, C.A. Carruthers, M.T. Wolf, S.P. Nagarkar, V. Agrawal, K.E. Jones, J. Kelly, S.A. Johnson, S.S. Velankar, S.C. Watkins, M. Modo, S.F. Badylak, Hydrogels derived from central nervous system extracellular matrix, Biomaterials 34 (2013) 1033–1040, https://doi.org/10.1016/j.biomaterials.2012.10.062.

[18] Y.R. Bai, B.Q. Lai, W.T. Han, J.H. Sun, G. Li, Y. Ding, X. Zeng, Y.H. Ma, Y.S. Zeng, Decellularized optic nerve functional scaffold transplant facilitates directional axon regeneration and remyelination in the injured white matter of the rat spinal cord, Neural Regen Philosophy and Phenomenological Research 16 (2021) 2276–2283, https://doi.org/10.4103/1673-5374.310696.

[19] J.D. Houle, V.J. Tom, D. Mayes, G. Wagoner, N. Phillips, J. Silver, Combining an autologous peripheral nervous system "bridge" and matrix modification by chondroitinase allows robust, functional regeneration beyond a hemisection lesion of the adult rat spinal cord, The Journal of Neuroscience 26 (2006) 7405–7415, https://doi.org/10.1523/JNEUROSCI.1166-06.2006.

[20] R.C. Cornelison, E.J. Gonzalez-Rothi, S.L. Porvasnik, S.M. Wellman, J.H. Park, D. D. Fuller, C.E. Schmidt, Injectable hydrogels of optimized acellular nerve for injection in the injured spinal cord, Biomedical Materials 13 (2018), https://doi.org/10.1088/1748-605X/aaab82.

[21] M.P. Côté, A. Hanna, M.A. Lemay, K. Ollivier-Lanvin, L. Santi, K. Miller, R. Monaghan, J.D. Houlé, Peripheral nerve grafts after cervical spinal cord injury in adult cats, Experimental Neurology 225 (2010) 173–182, https://doi.org/10.1016/j.expneurol.2010.06.011.

[22] Y. Xu, J. Zhou, C. Liu, S. Zhang, F. Gao, W. Guo, X. Sun, C. Zhang, H. Li, Z. Rao, S. Qiu, Q. Zhu, X. Liu, X. Guo, Z. Shao, Y. Bai, X. Zhang, D. Quan, Understanding the role of tissue-specific decellularized spinal cord matrix hydrogel for neural stem/progenitor cell microenvironment reconstruction and spinal cord injury, Biomaterials 268 (2021) 120596, https://doi.org/10.1016/j.biomaterials.2020.120596.

[23] D. Tukmachev, S. Forostyak, Z. Koci, K. Zaviskova, I. Vackova, K. Vyborny, I. Sandvig, A. Sandvig, C.J. Medberry, S.F. Badylak, E. Sykova, S. Kubinova, Injectable extracellular matrix hydrogels as scaffolds for spinal cord injury repair, Tissue Engineering – Part A 22 (2016) 306–317, https://doi.org/10.1089/ten.tea.2015.0422.

[24] I. Baek, Y. Song, Development of combinatorial therapeutics for spinal cord injury using stem cell delivery, JoVE (2024), https://doi.org/10.3791/66872 e66872.

[25] M. Lewis, G. David, D. Jacobs, P. Kuczwara, A.E. Woessner, J. Kim, K.P. Quinn, Y. Song, Materials today bio neuro-regenerative behavior of adipose-derived stem cells in aligned collagen I hydrogels, Materials Today Bio 22 (2023) 100762, https://doi.org/10.1016/j.mtbio.2023.100762.

[26] X. Shao, I.N. Taha, K.R. Clauser, Y. (Tom) Gao, A. Naba, MatrisomeDB: the ECM-protein knowledge database, Nucleic Acids Research 48 (2020) D1136–D1144, https://doi.org/10.1093/nar/gkz849.

[27] M. Ferrara, G. Lugano, M.T. Sandinha, V.R. Kearns, B. Geraghty, D.H.W. Steel, Biomechanical properties of retina and choroid: a comprehensive review of techniques and translational relevance, Eye 35 (2021) 1818–1832, https://doi.org/10.1038/s41433-021-01437-w.

[28] A. Sensini, L. Cristofolini, Biofabrication of electrospun scaffolds for the regeneration of tendons and ligaments, Materials (basel). 11 (2018) 1–43, https://doi.org/10.3390/ma11101963.

[29] Z. Feng, T. Kosawada, T. Nakamura, D. Sato, T. Kitajima, M. Umezu, Theoretical methods and models for mechanical properties of soft biomaterials, Aims Material Science 4 (2017) 680–705, https://doi.org/10.3934/matersci.2017.3.680.

[30] A.J. Engler, S. Sen, H.L. Sweeney, D.E. Discher, Matrix elasticity directs stem cell lineage specification, Cell 126 (2006) 677–689, https://doi.org/10.1016/j.cell.2006.06.044.

[31] C.A. Ribeiro, J.S. Fraga, M. Grãos, N.M. Neves, R.L. Reis, J.M. Gimble, N. Sousa, A. J. Salgado, The secretome of stem cells isolated from the adipose tissue and Wharton jelly acts differently on central nervous system derived cell populations, Stem Cell Research & Therapy 3 (2012), https://doi.org/10.1186/scrt109.

[32] A. Li, S. Dubey, M.L. Varney, B.J. Dave, R.K. Singh, IL-8 directly enhanced endothelial cell survival, proliferation, and matrix metalloproteinases production and regulated angiogenesis, Journal of Immunology 170 (2003) 3369–3376, https://doi.org/10.4049/jimmunol.170.6.3369.

[33] M. Nakamichi, Y. Akishima-Fukasawa, C. Fujisawa, T. Mikami, K. Onishi, Y. Akasaka, Basic fibroblast growth factor induces angiogenic properties of fibrocytes to stimulate vascular formation during wound healing, The American Journal of Pathology 186 (2016) 3203–3216, https://doi.org/10.1016/j.ajpath.2016.08.015.

[34] X. Xin, S. Yang, G. Ingle, C. Zlot, L. Rangell, J. Kowalski, R. Schwall, N. Ferrara, M. E. Gerritsen, Hepatocyte growth factor enhances vascular endothelial growth factor-induced angiogenesis in vitro and in vivo, The American Journal of Pathology 158 (2001) 1111–1120, https://doi.org/10.1016/S0002-9440(10)64058-8.
[35] E. Fagiani, G. Christofori, Angiopoietins in angiogenesis, Cancer Letters 328 (2013) 18–26, https://doi.org/10.1016/j.canlet.2012.08.018.
[36] N. Deznabi, S. Hosseini, M. Rajabi, Neurotrophic factors-based therapeutic strategies in the spinal cord injury: an overview of recent preclinical studies in rodent models, The Egyptian Journal of Neurology, Psychiatry and Neurosurgery 59 (2023), https://doi.org/10.1186/s41983-023-00661-3.
[37] N.I. Bamber, H. Li, X. Lu, M. Oudega, P. Aebischer, X.M. Xu, Neurotrophins BDNF and NT-3 promote axonal re-entry into the distal host spinal cord through Schwann cell-seeded mini-channels, The European Journal of Neuroscience 13 (2001) 257–268, https://doi.org/10.1111/j.1460-9568.2001.01387.x.
[38] X.Y. Song, F. Li, F.H. Zhang, J.H. Zhong, X.F. Zhou, Peripherally-derived BDNF promotes regeneration of ascending sensory neurons after spina cord injury, PLoS One1 3 (2008), https://doi.org/10.1371/journal.pone.0001707.
[39] A. Dravid, S.J. O'Carroll, D. Svirskis, Neurotrophins and their role in axonal outgrowth following spinal cord injury, Cellular, Molecular, Physiological, and Behavioral Aspects Spinal Cord Injury (2022) 215–227, https://doi.org/10.1016/b978-0-12-822427-4.00018-6.
[40] G. Paratcha, F. Ledda, GDNF and GFRα: a versatile molecular complex for developing neurons, Trends in Neurosciences 31 (2008) 384–391, https://doi.org/10.1016/j.tins.2008.05.003.
[41] H. Zhang, F. Wu, X. Kong, J. Yang, H. Chen, L. Deng, Y. Cheng, L. Ye, S. Zhu, X. Zhang, Z. Wang, H. Shi, X. Fu, X. Li, H. Xu, L. Lin, J. Xiao, Nerve growth factor improves functional recovery by inhibiting endoplasmic reticulum stress-induced neuronal apoptosis in rats with spinal cord injury, Journal of Translational Medicine 12 (2014) 1–15, https://doi.org/10.1186/1479-5876-12-130.
[42] M. Salinas, R. Diaz, N.G. Abraham, C.M.R. De Galarreta, A. Cuadrado, Nerve growth factor protects against 6-hydroxydopamine-induced oxidative stress by increasing expression of heme oxygenase-1 in a phosphatidylinositol 3-kinase-dependent manner, The Journal of Biological Chemistry 278 (2003) 13898–13904, https://doi.org/10.1074/jbc.M209164200.
[43] Y.H. Song, S.H. Shon, M. Shan, A.D. Stroock, C. Fischbach, Adipose-derived stem cells increase angiogenesis through matrix metalloproteinase-dependent collagen remodeling, Integrative Biology (United Kingdom) 8 (2016) 205–215, https://doi.org/10.1039/c5ib00277j.
[44] D. Lam, H.A. Enright, S.K.G. Peters, M.L. Moya, D.A. Soscia, J. Cadena, J. A. Alvarado, K.S. Kulp, E.K. Wheeler, N.O. Fischer, Optimizing cell encapsulation condition in ECM-Collagen I hydrogels to support 3D neuronal cultures, Journal of Neuroscience Methods 329 (2020) 108460, https://doi.org/10.1016/j.jneumeth.2019.108460.
[45] A.G. Marneros, B.R. Olsen, Physiological role of collagen XVIII and endostatin, The FASEB Journal 19 (2005) 716–728, https://doi.org/10.1096/fj.04-2134rev.
[46] N.U.B. Hansen, N. Willumsen, J.M.B. Sand, L. Larsen, M.A. Karsdal, D.J. Leeming, Type VIII collagen is elevated in diseases associated with angiogenesis and vascular remodeling, Clinical Biochemistry 49 (2016) 903–908, https://doi.org/10.1016/j.clinbiochem.2016.05.023.
[47] N.E.S. Sibinga, L.C. Foster, C.M. Hsieh, M.A. Perrella, W. Sen Lee, W.O. Endege, E. H. Sage, M.E. Lee, E. Haber, Collagen VIII is expressed by vascular smooth muscle cells in response to vascular injury, Circulation Research 80 (1997) 532–541, https://doi.org/10.1161/01.RES.80.4.532.
[48] J. Liauw, S. Hoang, M. Choi, C. Eroglu, M. Choi, G.H. Sun, M. Percy, B. Wildman-Tobriner, T. Bliss, R.G. Guzman, B.A. Barres, G.K. Steinberg, Thrombospondins 1 and 2 are necessary for synaptic plasticity and functional recovery after stroke, Journal of Cerebral Blood Flow and Metabolism 28 (2008) 1722–1732, https://doi.org/10.1038/jcbfm.2008.65.
[49] M.M. Krady, J. Zeng, J. Yu, S. MacLauchlan, E.A. Skokos, W. Tian, P. Bornstein, W. C. Sessa, T.R. Kyriakides, Thrombospondin-2 modulates extracellular matrix remodeling during physiological angiogenesis, The American Journal of Pathology 173 (2008) 879–891, https://doi.org/10.2353/ajpath.2008.080128.
[50] J.C. Xu, M.F. Xiao, I. Jakovcevski, E. Sivukhina, G. Hargus, Y.F. Cui, A. Irintchev, M. Schachner, C. Bernreuther, The extracellular matrix glycoprotein tenascin-R regulates neurogenesis during development and in the adult dentate gyrus of mice, Journal of Cell Science 127 (2014) 641–652, https://doi.org/10.1242/jcs.137612.
[51] C.H. Shih, M. Lacagnina, K. Leuer-Bisciotti, C. Pröschel, Astroglial-derived periostin promotes axonal regeneration after spinal cord injury, The Journal of Neuroscience 34 (2014) 2438–2443, https://doi.org/10.1523/JNEUROSCI.2947-13.2014.
[52] S.W.Y. Low, T.B. Connor, I.S. Kassem, D.M. Costakos, S.S. Chaurasia, Small Leucine-Rich Proteoglycans (SLRPs) in the Retina, (2021).
[53] A.N. Stratman, K.M. Malotte, R.D. Mahan, M.J. Davis, G.E. Davis, Pericyte recruitment during vasculogenic tube assembly stimulates endothelial basement membrane matrix formation, Blood 114 (2009) 5091–5101, https://doi.org/10.1182/blood-2009-05-222364.
[54] B.C. Searle, L.K. Pino, J.D. Egertson, Y.S. Ting, R.T. Lawrence, B.X. MacLean, J. Villén, M.J. MacCoss, Chromatogram libraries improve peptide detection and quantification by data independent acquisition mass spectrometry, Nature Communications 9 (2018), https://doi.org/10.1038/s41467-018-07454-w.
[55] S. Graw, J. Tang, M.K. Zafar, A.K. Byrd, C. Bolden, E.C. Peterson, S.D. Byrum, proteiNorm - A user-friendly tool for normalization and analysis of TMT and label-free protein quantification, ACS Omega 5 (2020) 25625–25633, https://doi.org/10.1021/acsomega.0c02564.
[56] W. Huber, A. von Heydebreck, H. Sültmann, A. Poustka, M. Vingron, Variance stabilization applied to microarray data calibration and to the quantification of differential expression, Bioinformatics 18 (2002) S96–S104, https://doi.org/10.1093/bioinformatics/18.suppl_1.S96.
[57] M.E. Ritchie, B. Phipson, D. Wu, Y. Hu, C.W. Law, W. Shi, G.K. Smyth, Limma powers differential expression analyses for RNA-sequencing and microarray studies, Nucleic Acids Research 43 (2015) e47.
[58] V.L. Cross, Y. Zheng, N. Won Choi, S.S. Verbridge, B.A. Sutermaster, L.J. Bonassar, C. Fischbach, A.D. Stroock, Dense type I collagen matrices that support cellular remodeling and microfabrication for studies of tumor angiogenesis and vasculogenesis in vitro, Biomaterials 31 (2010) 8596–8607, https://doi.org/10.1016/j.biomaterials.2010.07.072.
[59] J.N. Sleigh, S.J. West, G. Schiavo, A video protocol for rapid dissection of mouse dorsal root ganglia from defined spinal levels, BMC Research Notes 13 (2020) 4–9, https://doi.org/10.1186/s13104-020-05147-6.